Geoderma 440 (2023) 116708

Contents lists available at ScienceDirect

Geoderma

journal homepage: www.elsevier.com/locate/geoderma

Reconstruction of historical soil surfaces and estimation of soil erosion rates with mound measurements and UAV photogrammetry in Mediterranean olive groves

Francisco Lima [a,*], Rafael Blanco-Sepúlveda [a], Mikel Calle [b], Dionisio Andújar [c]

[a] Geographic Analysis Research Group, Department of Geography, University of Malaga, Teatinos Campus, 29071 Malaga, Spain
[b] Department of Geography and Geology, University of Turku, Turku, Turun Yliopisto 20014, Finland
[c] Centre for Automation and Robotics, Spanish National Research Council (CSIC), La Poveda, 28500 Arganda del Rey (Madrid), Spain

ARTICLE INFO

Handling Editor: B. Minasny

Keywords:
Unmanned aerial vehicle
Soil erosion rate
Mediterranean mountain
Olive groves
Tree mounds
Tillage
Water erosion
Structure-from-motion (SfM)

ABSTRACT

Soil water erosion is one of the most important environmental problems for the sustainability of Mediterranean olive groves on hillsides. Governments and public agencies recognize the need to control this process in order to improve soil conservation, especially in vulnerable areas. In the present study, a simple, inexpensive method using Structure-from-motion (SfM) and Unmanned Aerial Vehicle (UAV) technology was applied to quantify the soil loss rates provoked by water erosion and tillage in mountain olive groves, according to a reconstruction of their historical surface features. Specifically, the main study aims were: i) to quantify the historical soil loss in olive groves, by analysing residual tree mounds; ii) to consider how soil relief and management can influence the erosion process; iii) to determine the degree to which the proposed method achieves the above aims.

Analysis revealed a mean erosion rate in the study area of 127.69 t ha^{-1} $years^{-1}$, with a linear relationship between soil truncation and slope ($R^2 = 0.64$, $p < 0.001$). The highest soil loss rates (-1.67 ± 0.48 m) occurred in areas where the slopes were steepest (22.36 ± 4.46 %) and the longitudinal profile rectilinear. Erosion rates are determined not only by the slope, but also by its position and distance from the tree mound. This study highlights the need for differential management based on slope-feature considerations, in order to limit soil losses. Overall, the tool presented to support decision making provides an effective method for calculating erosion rates.

1. Introduction

Olive trees (*Olea europaea*) cover more than 11 million hectares worldwide in over 60 countries, but predominantly in the Mediterranean basin, which accounts for 93.44 % of this global extension. In this region, 55 % of the olive groves are located in Europe, especially in Spain, which is the main producing country, with 24.40 % of the world's surface area dedicated to the crop (FAOSTAT, 2016, INE, 2009).

The agricultural industrialization and market globalization that have taken place in recent decades (Kraushaar et al., 2014), coupled with the significant support provided by the EU Common Agricultural Policy (De Graaff and Eppink, 1999) and the opening up of new consumer markets (Scheidel and Krausmann, 2011) have led to: i) a significant increase in the cultivated area, which has mainly affected less suitable mountain lands, and ii) an intensification of the production process, through the introduction of machinery, the elimination of vegetation cover and the excessive use of tillage, among other factors (Infante-Amate, 2011). Taguas and Gómez (2015) identified the expansion of olive groves and the increased application of mechanization as the main reasons for the increased water erosion experienced by many soils in southern European countries. This form of land degradation is a major threat to agricultural sustainability worldwide, producing average global losses of 0.3 % of annual crop yields (FAO, 2015). The European Union, too, has identified erosion as a major threat to agricultural soils, highlighting its negative impact on crop yields (Papiernik et al., 2009), increased river sedimentation, reduced surface water quality (Berger et al., 2006) and greater frequency and intensity of muddy floods (Evrard et al., 2007). In Mediterranean regions, this erosive process has become more severe and extensive (Lizaga Villuendas et al., 2022), causing significant economic losses. For traditional mountain olive groves, Colombo et al. (2003) losses due to soil erosion are estimated at 42–72 euros ha^{-1} yr^{-1}, while Taguas and Gómez (2015) calculated losses of up to 100 euros ha^{-1} yr^{-1}

* Corresponding author.
E-mail addresses: lima@uma.es (F. Lima), rblanco@uma.es (R. Blanco-Sepúlveda), mcanav@utu.fi (M. Calle), d.andujar@csic.es (D. Andújar).

https://doi.org/10.1016/j.geoderma.2023.116708
Received 8 June 2023; Received in revised form 29 October 2023; Accepted 2 November 2023
Available online 16 November 2023

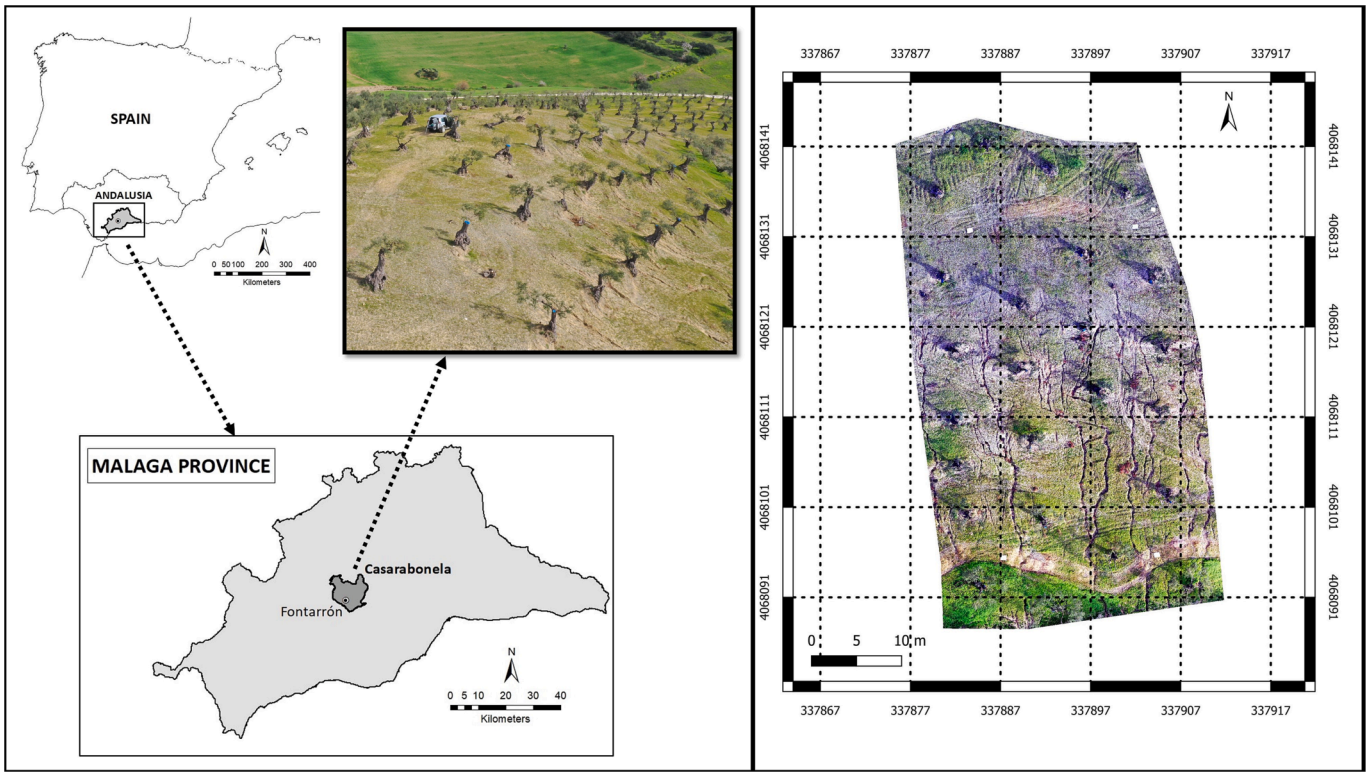

Fig. 1. Location map of the study site (Coordinate system: UTM Zone 30 N, datum ETRS 1989).

for the same cause. These costs and impacts of erosion are not limited to the boundaries of individual groves, but can also affect neighbouring lands and their infrastructure (Fernández et al., 2016).

Although soil water erosion is provoked by a complex combination of factors, agricultural management is the key to its control (Lima et al., 2018). For example, it has been shown that an inappropriate (i.e., non-contour) use of tillage accelerates erosion (Beniston et al., 2015), disturbing the soil and making it more susceptible to erosion and reduced fertility (Zhang et al., 2017). Moreover, tillage removes the protective plant cover and leaves the soil surface uncovered, which, together with commonly torrential Mediterranean rainfall and the steep slopes of some farmlands, produces high rates of soil erosion in mountain olive groves, sometimes exceeding 100 t ha^{-1} yr^{-1} (Vanwalleghem et al., 2010, 2011). In short, although the nature and danger of soil erosion are well known, the accurate, timely quantification of soil erosion rates is hampered by the large number of factors influencing this process (Lu et al., 2005). Various approaches have been taken to the study of soil erosion in agricultural lands, including those based on analyzing the spatial variability of soil topography, using a total station method (Ramos et al., 2008; Vanwalleghem et al., 2011), LIDAR data (Fernández et al., 2020), terrestrial laser scanning (Eitel et al., 2011; Bremer and Sass, 2012; Gao et al., 2021) or by measuring mounds (Vanwalleghem et al., 2010; Kraushaar et al., 2014). For each of these methods, unmanned aerial vehicles (UAVs) offer promising capabilities. Thus, structure-from-motion (SfM) and multi-view stereo (MVS) algorithms coupled with the use of UAVs are now commonly used for modelling complex landscapes on-demand, enabling high-resolution topographic change-detection studies to be conducted at minimal cost (Meinen and Robinson, 2020). A UAV equipped with an RGB camera is a non-destructive alternative that is less time consuming, and provides continuous, high-density sampling and continuous space coverage (Pineux et al., 2017). Its usefulness has been demonstrated at different scales and in various applications, from the detection of major landslides, badlands or gully erosion (Lucieer et al., 2014; Peter et al., 2014; Liu et al., 2016; Koci et al., 2017; Yang et al., 2019), to high-precision surface reconstruction, allowing the user to observe real runoff patterns and to model the relief changes that occur after major rainfall events (Pineux et al., 2017; Liu et al., 2019). However, the development of a fast, reliable methodology has yet to be perfected and if a method could be devised for measuring truncation and calculating soil erosion rates on cultivated slopes from the measurement of mounds by remote sensing, this would make the process speedier and more efficient and enable a greater area of land to be studied.

The method we propose for this purpose offers considerable temporal flexibility in data collection and facilitates periodic monitoring at the farm scale (covering the entire section of the slope from the upper drainage divide to the lower drainage line) without being too time-consuming, costly or destructive, in contrast to some alternatives that may require constant transit with heavy material over the study area, a factor that could even increase the erosion rate. In addition, another important methodological aspect is that it is a retrospective (historical) analysis methodology that improves the previous ones. DTM and UAV image comparison can only be used for the last few years, historical aerial images for the last 40–60 years, but this method can be applied to analyze a large interval of years. In this paper, we address the following aims related to the development of a truncation quantification method using UAVs: (i) to quantify the historical erosion rate in mountain olive groves, studying tree mounds using a method based on SfM-UAV technology; (ii) to analyze the influence of relief (hillside profile/slope gradient) and tillage on erosion rates through truncation; (iii) to evaluate the viability of this method for achieving the above aims.

2. Materials and methods

2.1. Study site and agricultural land management

The investigation was carried out in a commercial olive orchard known as Fontarrón, sited near the town of Casarabonela, in the province of Malaga (southern Spain). The study area consists of 5,500 m^2 on a hillside (central coordinates 4068114 W, 337918 N coordinate system

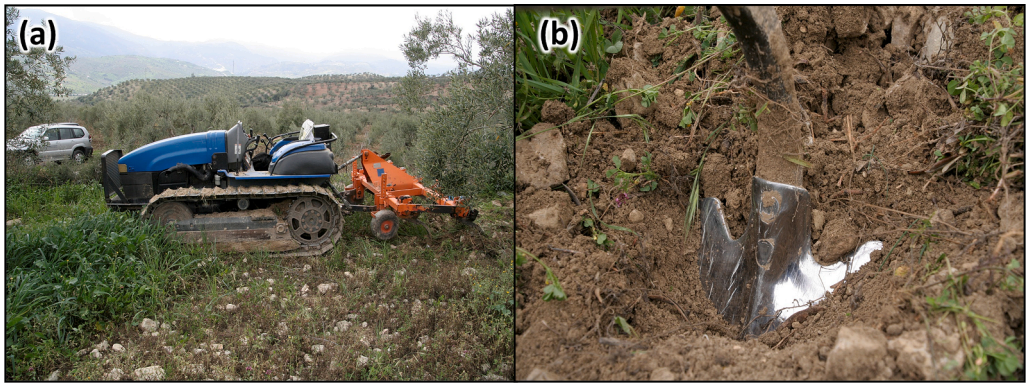

Fig. 2. Mechanised tillage tools: crawler tractor (a) equipped with a 2-row, 9-arm cultichisel type tool with duckfoot grids (b).

Fig. 3. General view of a field close to the study area, where the soil is bare.

UTM, Zone 30 N, datum ETRS89) (Fig. 1). The region has a temperate Mediterranean climate, with an average annual temperature of 18.4 °C and precipitation of 649 mm. According to the available historical series 1980–2022, the absolute annual maximum is 1606.1 mm and took place in the year 1989 This precipitation falls mainly from October to April, with the highest levels in November and December reaching absolute maximum values of 531 mm and 398 mm respectively. On average, rainfall occurs 46 days per year, and is often torrential. The absolute maximum in 24 h occurred in the year 2018 with 172 mm. Additional data on historical precipitation can be found in the appendix.

The predominant soils are Calcic Cambisols and Calcaric Regosols (FAO and IUSS, 2015), with an average depth of 66.4 ± 30.9 cm and an average organic carbon content of 20.3 ± 13.5 g kg^{-1}. The landscape is mainly characterized by sloping olive groves, with complex topographical conditions that vary from convex profiles at the top of the slope to concave ones at the bottom and rectilinear ones in the central area. The terrain is generally steep, but varies greatly, with slopes ranging from 2 to 24 %, with an average of 15.90 %. The olive trees are not irrigated and are set in a traditional square planting pattern 8–10 m apart. There are no terraces or indications of their past presence.

A conventional cultivation system is used, by which mechanised tillage is applied two or three times a year, breaking up the topsoil to improve water infiltration (Amami et al., 2021) and to remove spontaneous plant cover (Infante-Amate, 2011) without the use of herbicides. Tilling usually begins in January, after the fruit harvest, and is sporadically repeated until June. It is carried out with a crawler tractor (Fig. 2a) carrying a 2-row, 9-arm cultichisel-type tool equipped with duckfoot grids (Fig. 2b), commonly used in mountain olive groves.

As a result, the soil is bare for most of the year (Fig. 3). This gives rise to a predominance of erosion forms among which splash erosion (35.83 ± 15.65) and laminar erosion (46.39 ± 11.60) in soil disturbed by tools (Lima et al., 2018).

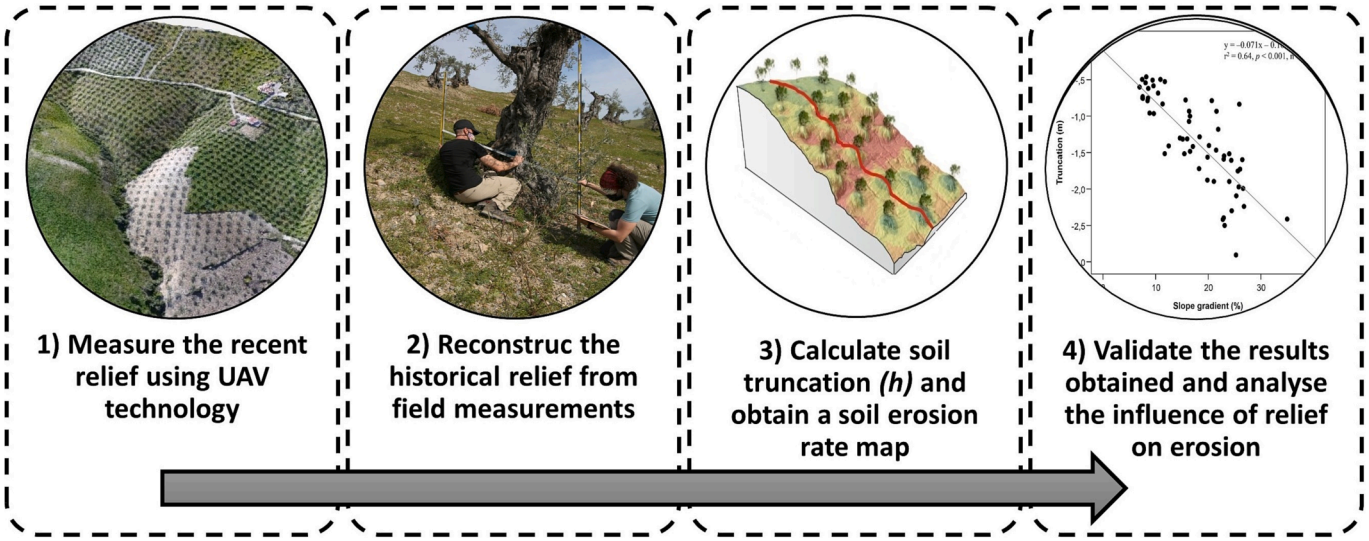

Fig. 4. Flowchart of the procedure for estimating historical soil loss rates in olive groves from tree mounds using UAV technology.

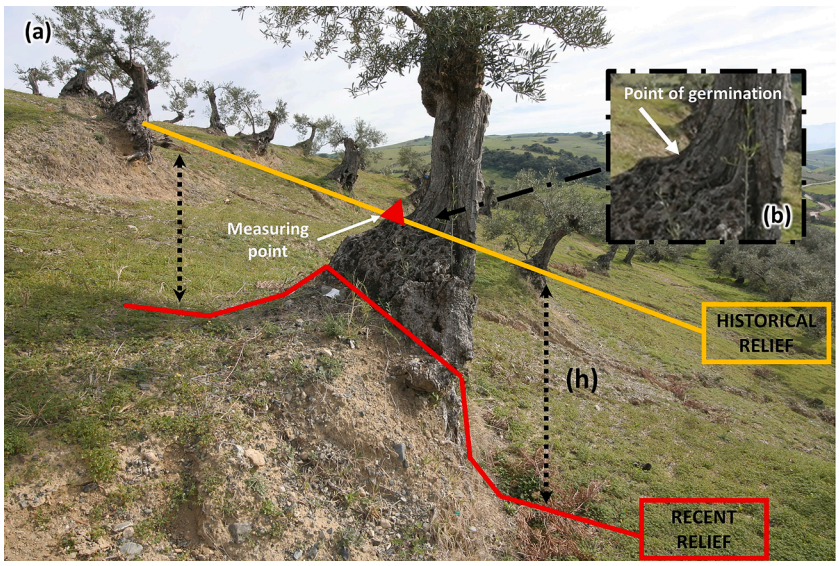

Fig. 5. Mound formed by erosion around a tree. The historical relief of the soil is indicated by the yellow line, while the red line indicates the position of the recent relief. The difference between the two surfaces corresponds to truncation *(h);* the eroded soil profile is represented by a dashed black line (a) and the point of germination is shown in detail (b). (For interpretation of the references to colour in this figure legend, the reader is referred to the web version of this article.)

In the study area, this soil management system originated in the 1960 s with the spread of mechanization (Lima et al., 2017, 2021). Until then, the normal practice was to perform one or two annual tillages with animal-drawn Roman ploughs. In most cases, the soil was cultivated with forage plants that protected it in the months of higher rainfall.

2.2. Study method

The full procedure for estimating historical soil loss rates in olive groves from tree mounds using SfM-UAV technology consists of four main phases (Fig. 4): 1) measure the recent relief using UAV technology; 2) reconstruct the historical relief from field measurements; 3) calculate soil truncation *(h)* and obtain a soil erosion rate map; 4) validate the results obtained and analyse the influence of relief on erosion.

2.2.1. Measure the recent relief using UAV technology

Various UAV flights were carried out during the winter, after the December tillage season that removed the vegetation cover from the soil. Thus, possible disturbances to the digital models were avoided, especially in the areas closest to the mounds.

The images were acquired using a commercial DJI Mavic 2 Pro quadcopter (DJI Ltd., Shenzhen, China) carrying a 1″ CMOS camera (DJI Ltd., Shenzhen, China). The flight altitude was 30 m and the image overlaps were high enough (72 % side-lap and 80 % forward-lap) to accurately construct the digital models.

Image mosaicking and digital model generation were performed with Pix4Dmapper Pro software, version 4.2.25 (Pix4D SA, Prilly, Switzerland), following a sequential process of image alignment, field geometry construction and orthophoto generation. The entire process was automatic, with the exception of the geolocation of four ground control points, which were taken in each survey field using a Trimble R2 global positioning system (RTK-GNSS) (Trimble GeoSpatial, Munich, Germany) with 10 mm horizontal and 20 mm vertical accuracy. The estimated accuracy of the ground control points can be found in the appendix section of this document.

Recent digital models have been generated by random triangulation following the Delaunay method. This method is the default method used by the Pix4d software and is recommended for agricultural fields and accumulations because it ensures that any point on the surface is as close as possible to a node. It is a method that has shown good results to quantify and map soil losses at field scale produced by extreme rainfall events from digital elevation models (Martínez-Casasnovas et al., 2002). The quality of the point cloud classification method has been high and the depth filtering aggressive.

As a result, an orthomosaic with ground sample distance (GSD) of 0.075 m was obtained, together with two digital models: i) Recent Digital Terrain Model (RDTM) and ii) Recent Digital Surface Model (RDSM), each with a GSD of 0.035 m. The difference between RDTM and RDSM was calculated in order to eliminate aerial structures (olive grove canopies) that might interfere with the results. Finally, the gradient for the entire slope was calculated from the RDTM.

2.2.2. Reconstruct the historical relief from field measurements

The typical microtopography of old olive groves is very suitable for the reconstruction of the historical ground surface level because individual trees are commonly located on a small mount or circular mound formed by erosion (Fig. 5a).

The historical relief was determined in the field using the procedure described by Vanwalleghem et al., (2010, 2011) and Kraushaar et al. (2014). This technique involves measuring the tree germination point (Fig. 5b), as an indicator of the historical relief existing when the grove was planted. As indicated by Bochet et al. (2000), soil mounds under trees can be formed by various processes, either cumulative or erosive. Water erosion leaves the mounds as remnants of the former soil surface. In addition to the above, tillage is the prevailing anthropogenic erosive factor (Vanwalleghem et al., 2010).

In order to cover the entire slope section from the upper drainage divide to the lower drainage line (which could be considered equivalent to a USLE type plot), the mound heights (germination point) of 24 trees were determined, using a Trimble R2 global positioning system (RTK-GNSS) (Trimble GeoSpatial, Munich, Germany).

The exact identification of the germination point was obtained following the observations of Kraushaar et al. (2014), who reported that olive grove roots in the soil have no bark, but once exposed to air, they develop a bark approximately 1 cm thick as protection from transpiration. Thus, measurements were taken 1 cm below the germination point to account for subsequent thickening of the bark, which produces a slightly higher germination point. The selection criteria included: i) visible signs of the uncovering of roots due to erosion; ii) the location of the germination point, where the trunk ends and the root begins.

Once the heights of 24 mounds were determined, the Historical Digital Terrain Model (HDTM) was reconstructed using ArcGIS 10.8

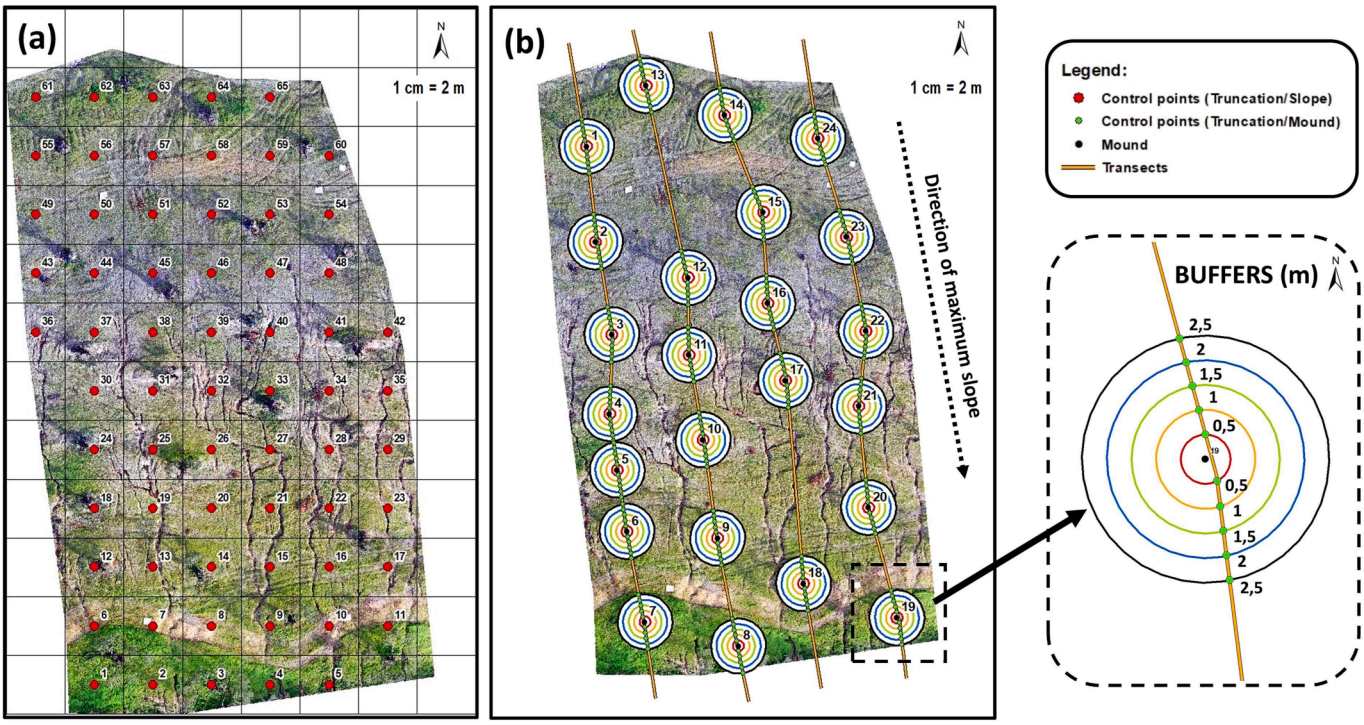

Fig. 6. Truncation data validation: with different slopes, hillside profiles (a) and position/proximity to the mound (b).

(Environmental Systems Research Institute, California, USA). For this purpose, the 80 % (19) of the mound heights were used for interpolation using the deterministic inverse distance weighting (IDW) method. The remaining 20 % (5) of the points were used to validate the interpolation result in the same software.

The difference between HDTM and RDTM was then calculated. Thus, a digital model was created with the same characteristics as the RDTM but at the level of the historical surface provided by the heights of the mounds. This procedure assumes that the historical microtopography of the terrain (HDTM) was similar to the current one (RDTM) but without the truncation effect.

2.2.3. *Calculate soil truncation (h) and obtain a soil erosion rate map*

The total truncation of the soil profile attributed to erosion since the establishment of the orchard was determined using the mounds as indicators of the decrease in surface area and expressed in linear meters/year. By subtracting the RDTM from the HDTM, we obtained a new digital model showing the loss of the surface horizon (truncation) in cubic metres. This was termed the Truncation Digital Terrain Model (TDTM). To obtain soil mass loss rates from volumetric data, 24 dry soil samples were taken around the mounds, and soil bulk density was determined using the core method (Blake and Hartge, 1986). These points were georeferenced with a global position system (RTK-GNSS) and transferred to ArcGIS 10.8 (Environmental Systems Research Institute, California, USA). Similarly to the creation of the HDTM, 80 % of the 24 dry soil samples were used to create a new bulk density (BD) raster layer for the whole study area. The IDW method was used for interpolation. The remaining 20 % of the points were used for validation. A 5 m square grid was created for the entire study area, with a point located at the centre of each grid, giving a total of 65 points. The bulk density data were extracted from the BD raster layer. Once the data was obtained, the mean and standard deviation were calculated for the sample segmented by hillslope profile (convex, rectilinear and concave).

According to interviews with local farmers, the age of the plantation was estimated at 115 years. The soil erosion rate was then calculated from the volume of soil erosion, the tree age and the bulk density, following Vanwalleghem et al. (2011), and the soil erosion rate map expressed in t/ha^{-1} years^{-1} was obtained.

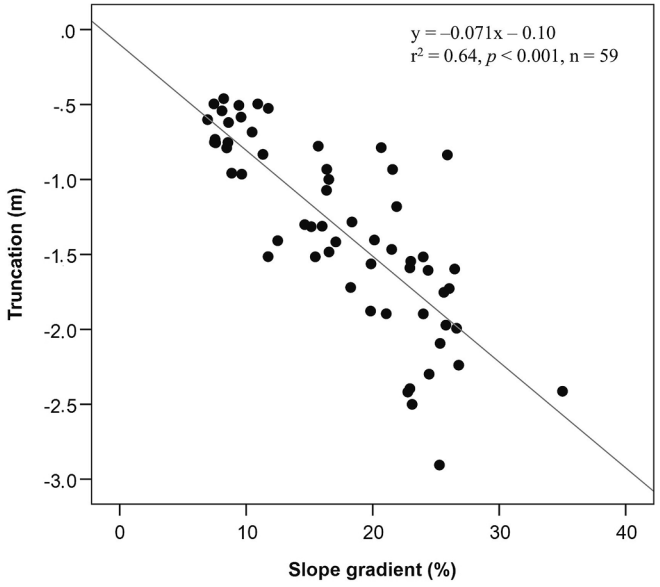

Fig. 7. Relationship between slope and soil truncation.

2.2.4. *Validate the results and analyse the influence of relief on erosion*

Soil truncation with slope was validated by locating 65 control points (truncation/slope) on the study slope (Fig. 6a). These points were created from the superposition of a 5 m side grid, at the central point of which truncation (TDTM), slope and hillside profile data were taken. The truncation behaviour in the proximity of the mounds, along the slope profile, was determined by assuming buffers at 0.5, 1, 1.5, 2 and 2.5 m around each of the 24 mounds within the study area. Subsequently, following the line of maximum slope, transects were drawn perpendicular to these buffers, resulting in 240 control points

Table 1
Truncation in relation to slope gradient and hillside profiles (convex, rectilinear and concave). Values: mean ± standard deviation (n = 65).

Hillside profiles	Abbreviation	Convex	Rectilinear	Concave
Slope gradient (m)	Slp	8.77 ± 1.28 a** b**	22.40 ± 4.46 a** c*	18.02 ± 4.68b** c*
Truncation (%)	T	−0.68 ± 0.16 d** e*	−1.76 ± 0.52 d** f*	−1.27 ± 0.38 e* f*

Note: For each hillside profiles, values followed by the same letters are significantly different (* $p < 0.01$, ** $p < 0.001$) according to Tukey's HSD test.

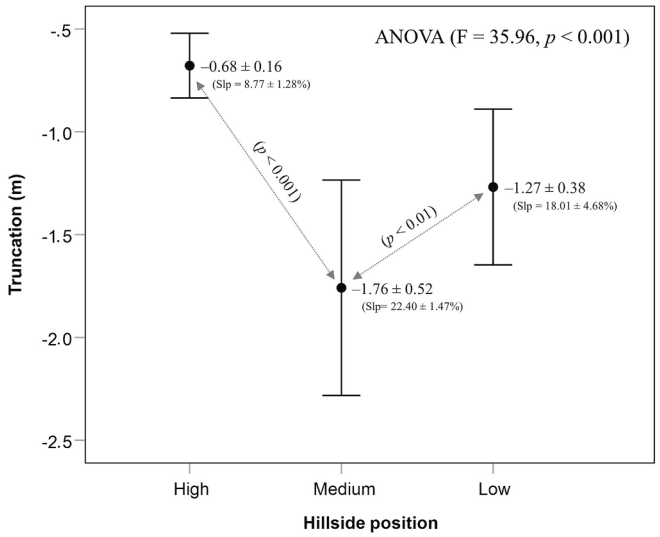

Fig. 8. Truncation in the convex, rectilinear and concave hillside profiles. Values: mean ± standard deviation (n = 65). ANOVA and significance level of Tukey's HSD test between the three types of hillside profile.

(truncation/mound) where TDTM and slope data were extracted, 120 at the top of the mound and another 120 at the bottom (Fig. 6b).

The relationship between TDTM and slope was determined by regression analysis. The difference in TDTM in the hillside profile (convex, rectilinear and concave) and its position/proximity to the mound (high and low/0.5, 1, 1.5, 2, 2.5) was determined by analysis of the variance (ANOVA) and by Tukey's honestly significant difference (HSD) test. All statistical analyses were performed with IBM SPSS Statistics 25.0.

3. Results

3.1. Evaluating the slope and truncation along the hillside profile (convex, rectilinear and concave)

Regression analysis showed a statistically significant relationship ($R^2 = 0.64$, $p < 0.001$) between soil truncation and slope (Fig. 7).

In addition, ANOVA revealed statistically significant differences (at 99 % confidence) between the three hillside profiles and truncation ($F = 35.96$, $p < 0.001$) (Table 1 and Fig. 8). The most significant truncation was observed in the rectilinear hillside profile (-1.76 ± 0.52 m), corresponding to the zone with the steepest slope (22.36 ± 4.46 %). In the slope zones with convex and concave profiles, the slopes are softened, with lower truncation values (-0.68 ± 0.16 and −1.27 ± 0.38 m respectively). Therefore, the data reflect a clear direct relationship between truncation, slope gradient and hillside profile.

Tukey's HSD test also revealed statistically significant differences between each of the hillside profiles: convex-rectilinear ($p < 0.001$), rectilinear-concave ($p < 0.01$) and convex-concave ($p < 0.01$) (Fig. 8).

3.2. Evaluation of truncation in the proximity of the mound (above and below the tree)

ANOVA revealed statistically significant differences (at 99 % confidence) between truncation and position/proximity to the mound in the

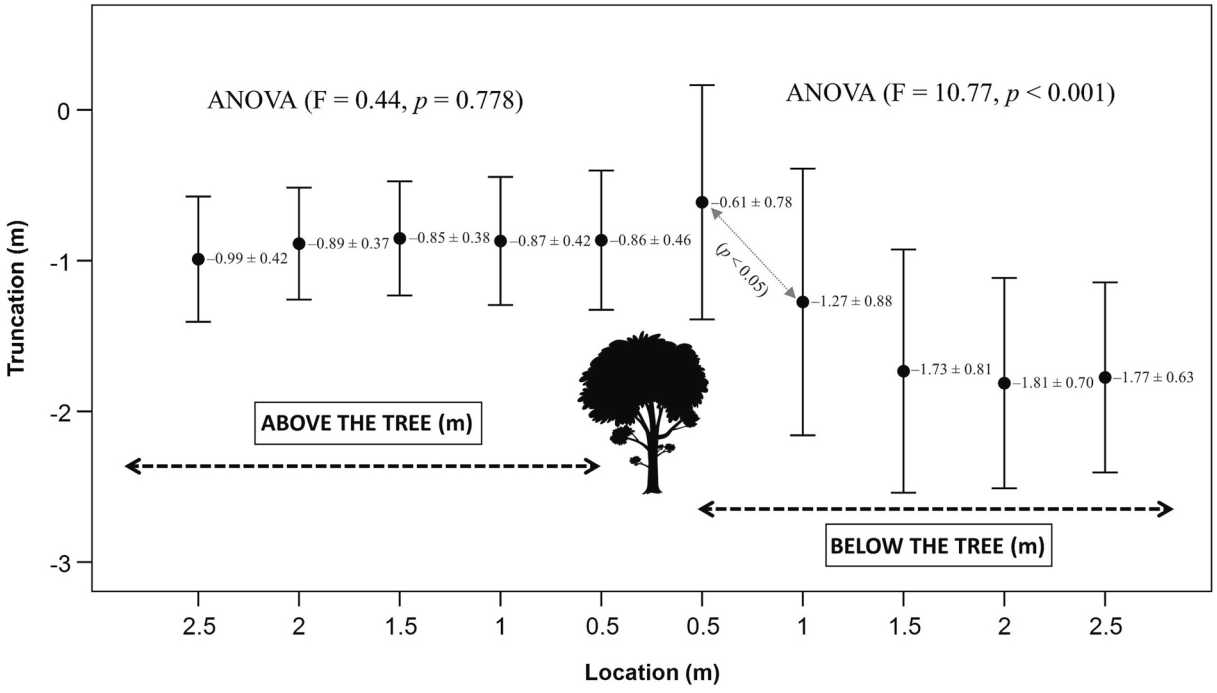

Fig. 9. Truncation in the areas above and below the tree. Values: mean ± standard deviation (n = 240). ANOVA and significance level of Tukey's HSD test between the types of position/proximity to the mound. Non-significant differences are not marked.

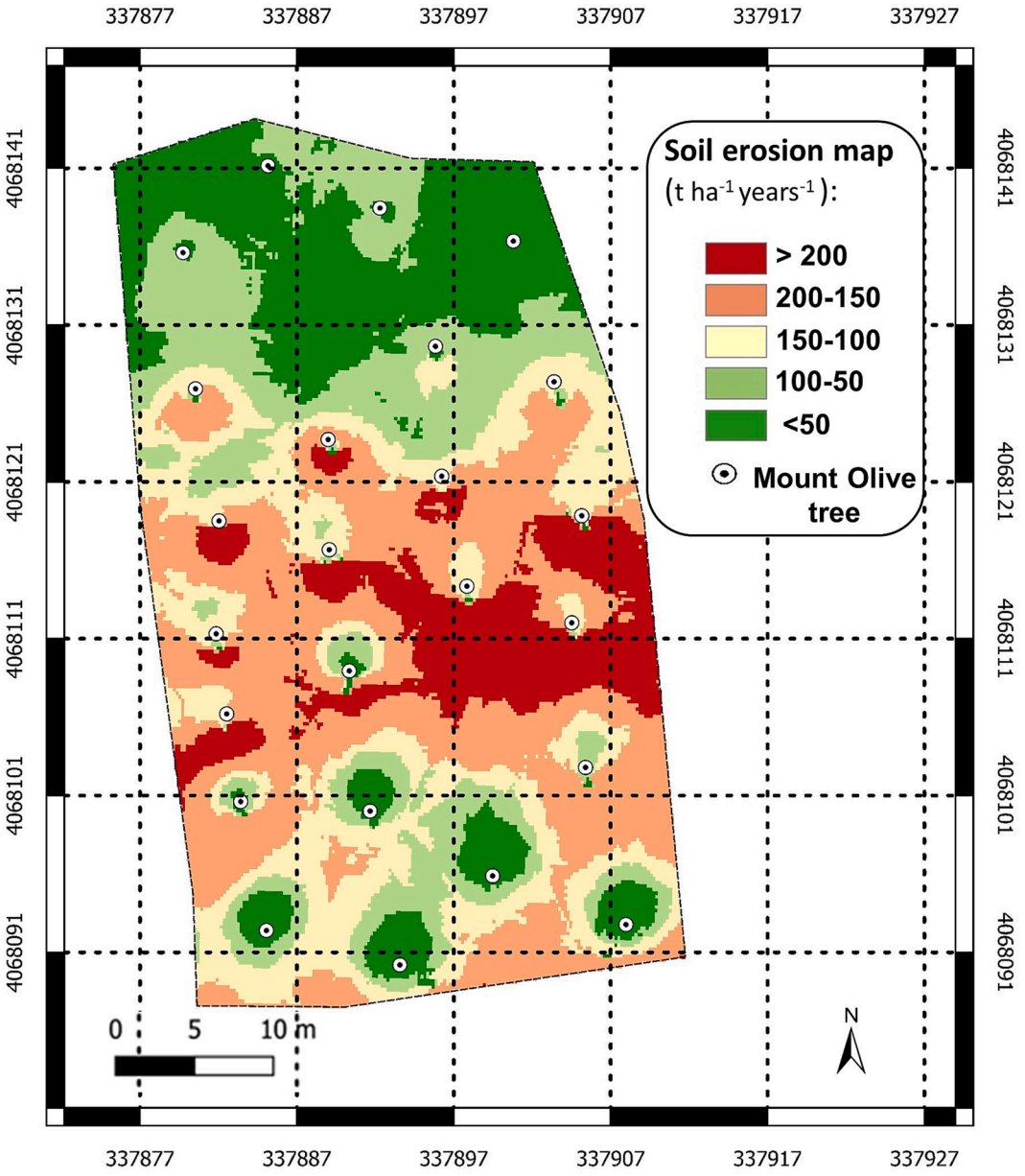

Fig. 10. Map of soil erosion rate in the study area.

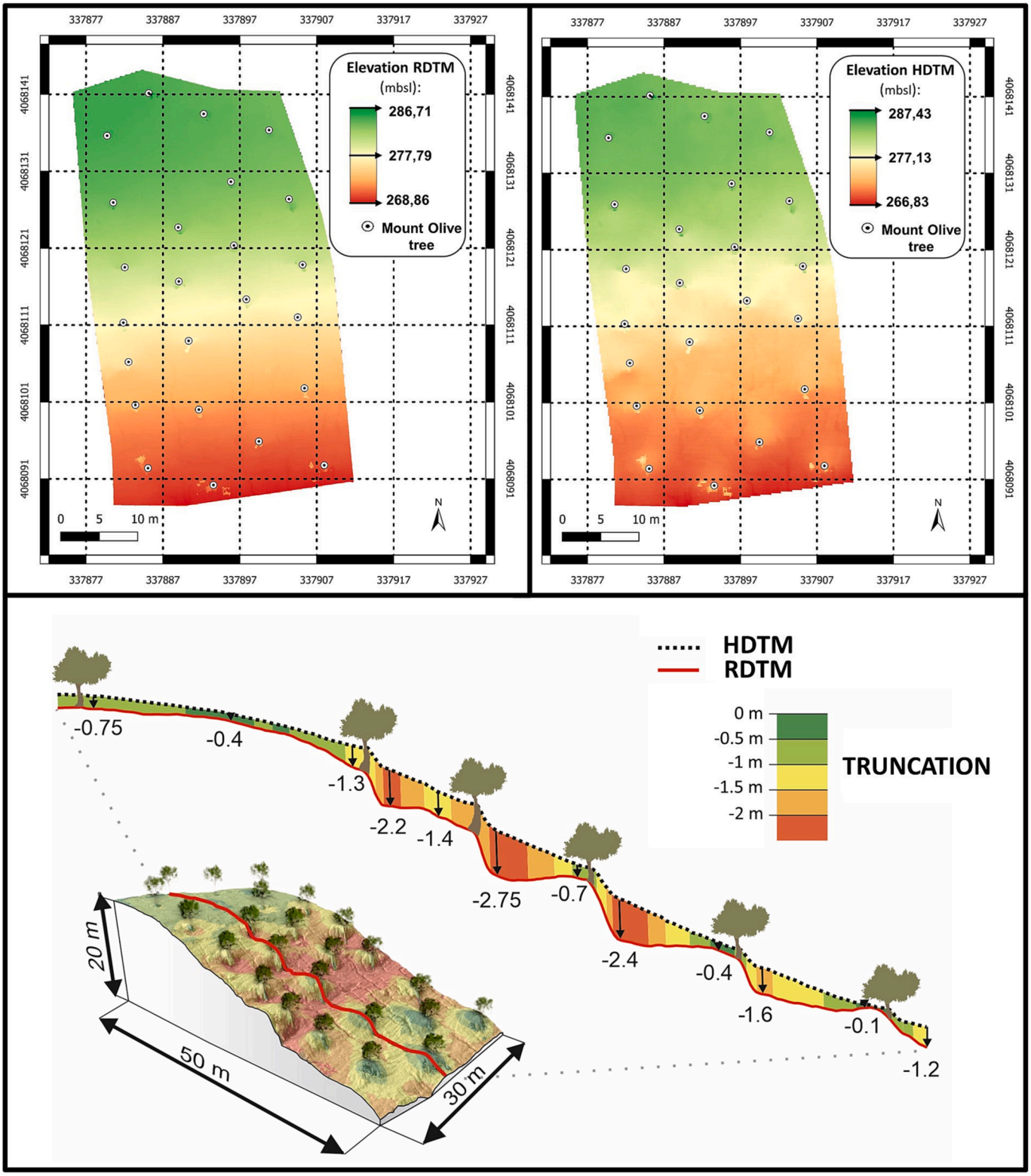

Fig. 11. Digital Terrain Models and transverse profile of the truncation along the slope.

area below the tree ($F = 10.77$, $p < 0.001$). However, the same was not true for the area above the tree ($F = 0.44$, $p = 0.778$) (Fig. 9).

Tukey's HSD test highlighted statistically significant differences ($p < 0.05$) between the locations below the tree closest to the mound (at 0.5 and 1 m) and its truncation (between -0.61 ± 0.78 and -1.27 ± 0.88 respectively). These differences ceased to be statistically significant with greater distance from the mound (>1.5 m). In this area, the truncation progressively increased up to 2 m away from the mound, where it reached -1.81 ± 0.70. From this point on, the truncation decreased slightly (-1.77 ± 0.63). However, above the tree, there was no great increase in truncation -0.86 ± 0.46, -0.87 ± 0.42, -0.85 ± 0.38 in the areas closest to the mound (at 0.5, 1 and 1.5 m, respectively). On the other hand, the truncation increased in the areas farther away from the mound (>1.5 m), with values of -0.99 ± 0.42 and -0.89 ± 0.37 at 2.5 and 2 m, respectively (Fig. 9).

3.3. Soil erosion rate map and evaluation of the digital models

The above procedure obtained an accurate soil erosion rate map, with a spatial resolution of 3.5 cm (Fig. 10), reflecting a total average erosion rate for the study area of 127.69 t ha^{-1} $years^{-1}$.

The distribution of erosion along the slope profile is clearly shown in the map. Erosion rates were more pronounced on the rectilinear part of the hillside (>200 t ha^{-1} $years^{-1}$), with an average bulk densities of 1.14 ± 0.056 g cm^{-3}. Where the slope was steeper (21–24 %) and the consequences of tillage more evident. In addition, a clear dissymmetry was observed between the area over the trees (less eroded) and the area below the trees (more eroded). The map also shows zones with lower erosion rates (<50 and 50–100 t ha^{-1} $years^{-1}$), corresponding to: i) areas where the slopes are less steep (0—11 %) (upper part of the slope with a convex profile) with an average bulk densities of 1.13 ± 0.062 g cm^{-3}, or ii) the area where soil deposition processes predominate are the lower (concave) part of the slope. The latter are found in the proximities of the mounds, especially in the upper part of the mounds, and also in the lower part of the slope (final section, concave profile), where the average bulk density is 1.10 ± 0.051 g cm^{-3} and the slope is slightly reduced (11–14 %), which facilitates the deposition of material from the higher areas. These outcomes are clearly shown in the cross-sectional profile of the slope (Fig. 11).

Applied interpolation methods allowed the consolidation of robust digital models (Fig. 11). The Delaunay triangulation method used in high-precision photogrammetry resulted in a reprojection of the RDTM with RMSE of 0.41. While the IDW method employed for HDTM reprojection showed an RMSE = 0.31 m, with a validation error of −0.29 ± 0.45 m. For the BD raster the RMSE = 0.11 m with a validation error of 0.005 ± 0.07 m.

4. Discussion

The historical soil loss in the study area is 127.69 t $ha^{-1}year^{-1}$, which is in line with the rates obtained in studies of other Mediterranean olive grove mountain regions, using similar methodologies based on the measurement of mound height. Comparable values include the 95 ± 8 t ha^{-1} $year^{-1}$ reported by Kraushaar et al. (2014) from a study conducted in Jordan, the 184 t ha^{-1} $year^{-1}$ measured by Vanwalleghem et al. (2010) in Cordoba (Southern Spain) and the 124 t ha^{-1} $year^{-1}$ that Vanwalleghem et al. (2011) concluded was the maximum rate for the periods of greatest historical erosion of the Andalusian Mediterranean olive grove. On the other hand, our study value is somewhat higher than the 81 t $ha^{-1}year^{-1}$ obtained for runoff plots by Bruggemann et al. (2005) in NW Syria.

The erosion value obtained in the present investigation is much higher than the 80 t ha^{-1} $year^{-1}$ which has frequently been cited as the average soil loss rate for Andalusian olive groves. However, the latter rate is based on an estimation of the USLE model of López-Cuervo (1990), and does not take into account in-field sedimentation. Therefore, Gómez et al. (2005) and Fleskens and Stroosnijder (2007), among others, have observed that this value could be erroneous.

In any case, the erosion rates we present are higher than the soil renewal rates by weathering and dust input of 0.3–1.4 t ha^{-1} $year^{-1}$ that authors such as Verheijen et al. (2009) indicate for Europe. Moreover, they are also higher than the much higher threshold used by Gómez et al. (2003) for Spain, of 8.4 to 11.4 t ha^{-1} $year^{-1}$.

There is evident disagreement in the literature regarding estimates of soil loss rates, probably due to the diverse orchard characteristics considered, methods employed and scales of analysis employed (Fleskens and Stroosnijder, 2007). However, our study results are within the range of findings obtained previously with similar methodologies, indicating the usefulness of our approach as an agile, effective means of determining erosion rates in Mediterranean mountain olive groves with specific characteristics. Furthermore, our study findings contribute to the development of effective soil erosion control policies, a necessary component of the EU's Common Agricultural Policy (Lima, 2022).

Regarding the behaviour of erosion rates along the slope, our results show there is a linear relationship between soil truncation and slope ($R^2 = 0.64$, $p < 0.001$). The highest rates of soil truncation (-1.67 ± 0.48 m) were observed in the areas with the steepest slopes (22.36 ± 4.46 %). This result corroborates Kraushaar et al. (2014), who showed that the depth of truncation increased to −0.41 m in areas of steepest slope (≥70 %), while declinations from 0 % to 38 % and from 38 % to 70 % had lower truncation values, ranging from −0.14 to −0.35 m and from −0.31 to −0.34 m, respectively.

As concerns the hillside profile, erosion rates were clearly greater in the rectilinear part, coinciding with the transit zone from a convex to a concave profile (i.e., above the concave profile). Although the slope topography is modified by anthropogenic action, we concur with Van Oost et al. (2005) in that, generally, erosion has greatest impact above the concave edge, where runoff attains the highest level of transport energy.

Soil erosion rates not only increase with slope, but are also influenced by the position and distance from the mound. Thus, there is a clear relationship between truncation and the lower areas of the mounds (under the tree) ($F = 10.77$, $p < 0.001$), which present an evident dissymmetry in comparison with the upper areas (above the tree). In the lower areas, the truncation increased rapidly in the first few metres and progressively up to 2 m away from the mound, at which point it began to descend (on the high area of the adjacent down-slope mound). In the upper zones, truncation did not increase more markedly until a distance of 2 m from the mound (on the lower zone of the adjacent uphill mound). This behaviour is largely due to the modelling effects of tillage and runoff, as observed previously by Vanwalleghem et al. (2010) and Kraushaar et al. (2014). However, the presence of the mound is also a significant element of sediment retention and channelling of runoff.

For centuries, weeds have been controlled in the study area by means of tillage, first by animal traction and then by mechanical traction (Lima et al., 2017). Unfortunately, the alternate soil movements caused by this

tillage alter the soil structure, making it more susceptible to degradation (Zhang et al., 2017) and to erosive effects, especially in areas of greater slope (Zhang et al., 2019). Over the last 60 years, farming methods based on tillage that is both frequent (2 or 3 ploughing passes per year) and deep (>15 cm), have generated furrows and gullies that surround and define the mounds. Water erosion has been concentrated in these features, aggravated by torrential Mediterranean rainfall and by a conventional farming system that keeps the soil bare most of the year (Lima et al., 2018). In consequence, there has been significant soil loss, undermining and exposing the roots of the olive trees.

Continued tillage has resulted in a hidden terracing along the crop lines transverse to the slope which, in the areas between trees, has been dismantled by concentrated surface runoff, while in the areas near the mounds it is maintained. The mound, with its root system, retains sediments and breaks the general continuity of the slope, creating microtopographic structures in the upper zones of the mounds. A similar pattern of erosion has been reported by Bochet et al. (2000) and Gyssels et al. (2005) in their studies of Mediterranean shrublands. Thus, in the upper areas of the mounds, the erosion caused by ploughing and runoff is compensated by the contribution of sediments received from uphill areas, which are retained and accumulated by the mound itself. In contrast, in the lower areas of the mounds, the areas located closest to the mound are severely affected by erosion from tillage and from the runoff surrounding and defining the mound (Vanwalleghem et al., 2010; Kraushaar et al., 2014). This outcome, together with the non-reception of sediment from the uplands (due to interception by the mound) generates high erosion rates and hence significant truncation in the area.

Nowadays, GIS software integrates different interpolation algorithms that allow the creation of continuous surfaces from discrete points. Inverse distance weighting (IDW), natural neighbour (NN), ordinary kriging (OK), and topo to raster (ANUDEM) are well known methods (Erdogan, 2009; Falivene et al., 2010; Li and Heap, 2014; Wise, 2007). Each method has advantages and disadvantages, and none performs better than the others in all landscapes (Agüera-Vega et al., 2020; Habib, 2021; Chen et al., 2022). The present work has shown how IDW is a useful method to interpolate field data and create 3D models with accurate results. IDW generated good predictions. These results are similar to those obtained by authors such as Lu and Wong (2008), Wong (2017) and Pereira et al. (2022), reconstructing models at high accuracy.

The RMSE values obtained in this work are in line with those reported in the literature. This is the case of the RMSE = 0.339 that authors such as Chen et al. (2022) show with the application of IDW for the reprojection of accurate digital terrain models, and somewhat higher RMSE = 0.220 obtained by Mancini et al. (2013) applying similar technology (UAV-SFM). Thus, it is stated that the RDTM obtained was created from current high-resolution surface data, while the data from which the HDTM is generated come from interpolations of a limited number of observations. This will depend on the number of existing field references (mounds). In addition, the horizontal accuracy of UAV photogrammetry is slightly better than the vertical accuracy, except in the case of extremely steep topography (Agüera-Vega et al., 2018). Many authors pointed out that the accuracy, measured in GSD values, was lower on flat surfaces than in complex topography (Jiménez-Jiménez et al., 2021). However, Mancini et al. (2013) using the UAV-based approach proved to be straightforward and the accuracy of the vertical dataset was comparable to the results obtained with terrestrial laser scanning technology (TLS).

In short, the analytical method described in this paper achieves the aims proposed. The SfM-UAV produces accurate digital surface models, clearly revealing mound morphology and erosional signs, and enabling truncation and historical soil loss rates to be quantified and mapped appropriately. Analysis of these layers of information reveals the erosive patterns of both runoff and deposition, and identifies those areas where soil loss is greatest and where corrective measures are needed.

5. Conclusions

This paper addresses the challenge of using remote sensing to assess the impact of agricultural activities in risk situations related to soil conservation. The results obtained demonstrate the capability of ultra-high resolution remote imagery acquired with UAV technology and analyzed with SfM techniques to quantify historical soil loss rates in Mediterranean mountain olive groves and thus produce hillside-scale soil erosion maps. The procedure employed successfully reconstructed the historical ground surface from measurements taken at the tree mounds, and determined, with cm-scale precision, the truncation of the current surface with respect to the historical surface on a complex hillside with different slope gradients and hillside profiles (convex, rectilinear and concave). The erosion rate observed is higher than the average reported in previous studies of Andalusian olive groves, although close to those obtained for other Mediterranean areas with methodologies based on the measurement of the mound. The study method revealed a significant relationship between truncation, slope gradient, hillside profile and proximity to the mound below the tree. Rates of soil loss were highest where slopes were steepest, where the hillside profile was rectilinear and where the location was close to the mound above the tree. The method described is simple to apply, enabling the practitioner to rapidly and accurately quantify soil loss rates, considering all the factors responsible for and/or consequent to the erosive process (erosion/deposition), over an appropriate time period and at an adequate scale. We suggest this approach could alleviate the lack of field data due to the calibration and validation problems that may be encountered with traditional models of soil erosion. Furthermore, it could provide governments and public administrations with accurate soil conservation information to help them define and apply effective measures of erosion control.

A final observation is the fact that the results of this work correspond to specific scale conditions in a crop characteristic of the Mediterranean mountains. Future research will be necessary to verify the response of the method at different scales, segmented according to the different types of erosion and in different agricultural scenarios. Furthermore, within the possibilities offered by reproducing historical surfaces where obtaining true ground data is complex, further experimentation on the different existing interpolation processes will be carried out in order to further improve the interpolated models.

Funding

This research has been funded by the OAPN under grant 2924S/2022, by the AEI under grants TED2021-130031B-I00 and PID2020-437113229RBC43/AEI/https://doi.org/10.13039/501100011033 and by the University of Malaga by grant B.1 of its own Research and Transfer Plan (B1-2022_19).

Declaration of Competing Interest

The authors declare that they have no known competing financial interests or personal relationships that could have appeared to influence the work reported in this paper.

Data availability

Data will be made available on request.

Acknowledgments

Thanks are due for the invaluable collaboration of the farmers of the Bajo Guadalhorce-Sierra de las Nieves Valley and to José Manuel Peña Barragán for providing the GPS instrumentation for the field measurements.

Appendix A

Table A1
Historical series of total monthly and annual precipitation. From 1980 to 2022.

Years	Oct.	Nov.	Dec.	Jan.	Febr.	Mar.	Apr.	May	Jun.	Jul.	Aug.	Sep.	TotalAnual (mm)
80–81	31	119	4	1	24	11	96	5	10	–	35	9	**343.6**
81–82	4	–	112	137	51	38	57	38	–	11	–	–	**448.7**
82–83	16	221	18	2	41	13	17	–	–	–	–	2	**328.6**
83–84	10	381	86	–	110	78	15	74	2	–	–	–	**755.4**
84–85	17	207	17	74	82	2	21	36	–	–	–	3	**458.2**
85–86	–	84	72	22	83	78	49	19	26	–	–	18	**451.8**
86–87	105	75	8	134	57	2	12	1	–	4	103	8	**509**
87–88	84	121	183	101	59	18	16	27	25	–	–	85	**717.9**
88–89	74	201	–	144	177	17	65	32	1	–	0	29	**740**
89–90	273	531	398	68	–	148	175	1	0	–	1	12	**1606.1**
90–91	70	107	88	8	118	138	87	10	11	–	–	30	**665.6**
91–92	178	40	69	36	119	42	29	1	127	–	–	14	**654.2**
92–93	91	12	48	72	77	77	28	58	6	–	0	2	**471**
93–94	146	126	0	46	76	17	48	12	1	–	0	–	**472.1**
94–95	55	39	5	16	14	23	9.5	3.3	18	2	–	–	**183.2**
95–96	–	75	332	333	118	87	21	121	–	–	23	31	**1140.7**
96–97	45	63	449	287	–	–	13	75	6	–	4	245	**1185.4**
97–98	73	147	171	116	222	10	12	67	14.3	–	0	19	**851.4**
98–99	–	106	93	39	29	58	25	9	3.2	–	2	25	**388.9**
99–00	110	26	40	140	–	17	196	71	3	–	–	3	**603.6**
00–01	44	36	204	68	48	71	3	37	–	3	–	122	**636.8**
01–02	78	88	178	23	19	95	50	3	1	–	0	19	**553.7**
02–03	43	96	84	28	90	91	45	5	–	1	–	8	**489.2**
03–04	233	109	202	8	141	140	39	76	–	–	–	2	**949.6**
04–05	40	85	67	4	117	68	9	16	–	–	2	2	**409.6**
05–06	60	33	19	146	62	101	28	22	34	–	5	12	**521.4**
06–07	61	176	25	38	48	9	95	52	–	–	3	124	**630.7**
07–08	73	22	169	36	80	34	76	17	–	–	–	238	**746**
08–09	159	70	98	47	87	55	45	8	16	–	–	83	**668.1**
09–10	15	19	334	257	293	215	182	8	10	0	32	34	**1398.1**
10–11	36	115	305	95	31	208	96	50	3	–	–	2	**940.1**
11–12	95	189	3	18	15	4	39	15	–	3	0	134	**516.7**
12–13	147	249	8	42	125	183	32	14	–	–	5	14	**819.2**
13–14	9	8	64	44	52	15	45	56	12	–	–	129	**431.7**
14–15	38	147	8	45	41	100	30	36	1	–	1	76	**523.4**
15–16	120	42	1	66	44	20	44	117	0	1	–	–	**453.1**
16–17	24	176	241	19	92	66	147	9	0	–	15	2	**790.9**
17–18	76	41	15	44	51	213	93	14	13	–	–	41	**601.2**
18–19	286	88	2	7	22	24	32	0	–	–	–	99	**560.2**
19–20	2	37	61	93	6	117	73	68	2	1	1	17	**476.9**
20–21	39	144	30	174	18	74	42	9	7	–	0	47	**583**
21–22	2	17	62	16.2	6	364	80	20	–	–	6	6	**579.3**
M*	***72.9***	***111.1***	***104.1***	***73.6***	***70.1***	***74.7***	***55.1***	***31.2***	***8.3***	***0.6***	***5.6***	***41.5***	***649***

M* Average monthly rainfall totals **Source:** Comisaría de aguas del sur de España, Servicio de hidrología. Provided by the observer Mr. Miguel Arjona.

Table A2
Historical series of maximums (1st, 2nd and 3rd) in 24 h. From 1980 to 2022.

Years	Maximum daily rainfall values		
	1	2	3
80–81	41.5	34.5	30.5
81–82	43.5	40	26.3
82–83	120	35	28
83–84	93.3	92	73
84–85	77	41	34.3
85–86	28.5	28.2	26.8
86–87	57.5	42.2	38
87–88	82	67	63.5
88–89	12.5	74.5	48
89–90	143.5	115.3	87.5
90–91	86.5	65.5	56
91–92	79.2	71	44.5
92–93	44.5	37	32.8
93–94	63	40.5	33.3
94–95	35	28	15.8
95–96	137.1	79.4	72.6
96–97	111	84.4	59.6
97–98	78.8	77.2	61.4
98–99	70	42	36.2
99–00	63	51	40.7
00–01	81.7	46	42
01–02	50.1	38.3	37
02–03	36.3	34	28.5
03–04	77.5	57.2	52.5
04–05	70.1	44.2	33
	49	29.1	27.5
06–07	79.8	63	40.5
07–08	102.5	73.2	46.9
08–09	52.2	45.5	44.8
09–10	89	71	70.9
10–11	87	74.8	55.6
11–12	102	58.2	47
12–13	61	59	58
13–14	85	52.2	36
14–15	60.4	44	27.1
15–16	47.5	41.5	33.7
16–17	124	98	76
17–18	45	43.8	39.3
18–19	172	73	33
19–20	34	33	30
20–21	74	58.5	56
21–22	87	53	48

Source: Comisaría de aguas del sur de España, Servicio de hidrología. Provided by the observer Mr. Miguel Arjona.

Table A3
Estimated accuracy of ground control points.

Label	XY error (m)	Z error (m)	Error (m)	Error (Pix)
GCP 1	0.17156	−0.00936969	0.171816	1.087
GCP 2	0.140532	−0.0356597	0.144986	1.098
GCP 3	0.169597	0.0347111	0.173113	1.080
GCP 4	0.181401	0.0101118	0.181682	0.765
TOTAL	**0.166472**	**0.0258192**	**0.168462**	**1.002**

References

Agüera-Vega, F., Carvajal-Ramírez, F., Martínez-Carricondo, P., Sánchez-Hermosilla López, J., Mesas-Carrascosa, F.J., García-Ferrer, A., Pérez-Porras, F.J., 2018. Reconstruction of extreme topography from UAV structure from motion photogrammetry. Meas. J. Int. Meas. Confed. 121, 127–128.

Agüera-Vega, F., Agüera-Puntas, M., Martínez-Carricondo, P., Mancini, F., Carvajal, F., 2020. Effects of point cloud density, interpolation method and grid size on derived Digital Terrain Model accuracy at micro topography level. Int. J. Remote Sens. 41, 8281–8299. https://doi.org/10.1080/01431161.2020.1771788.

Amami, R., Ibrahimi, K., Sher, F., Milham, P., Ghazouani, H., Chehaibi, S., Hussain, Z., Iqbal, H.M.N., 2021. Impacts of different tillage practices on soil water infiltration for sustainable agriculture. Sustainability 13, 3155. https://doi.org/10.3390/su13063155.

Beniston, J.W., Shipitalo, M.J., Lal, R., Dayton, E.A., Hopkins, D.W., Jones, F., Joynes, A., Dungait, J.a.J., 2015. Carbon and macronutrient losses during accelerated erosion under different tillage and residue management. Eur. J. Soil Sci. 66, 218–225. https://doi.org/10.1111/ejss.12205.

Berger, G., Kaechele, H., Pfeffer, H., 2006. The greening of the European common agricultural policy by linking the European-wide obligation of set-aside with voluntary agri-environmental measures on a regional scale. Environ Sci Policy 9, 509–524. https://doi.org/10.1016/j.envsci.2006.05.006.

Blake, G.R., and Hartge, K.H. 1986. Bulk density. In: L. Page, R.H. Miller, and D.R. Keeney (ed.) Methods of soil analysis. Part I. Physical and mineralogical methods. Second Edition. Agronomy. Madison. Wisconsin, USA. 9:363-375.

Bochet, E., Poesen, J., Rubio, J.L., 2000. Mound development as an interaction of individual plants with soil, water erosion and sedimentation processes on slopes. Earth Surf. Proc. Land. 25, 847–867. https://doi.org/10.1002/1096-9837(200008)25:8<847:AID-ESP103>3.0.CO;2-Q.

Bremer, M., Sass, O., 2012. Combining airborne and terrestrial laser scanning for quantifying erosion and deposition by a debris flow event. Geomorphology 138, 49–60. https://doi.org/10.1016/j.geomorph.2011.08.024.

Bruggemann, A., Masri, Z., Turkelboom, F., 2005. Strategies to sustain productivity of olive groves on steep slopes in the northwest of the Syrian Arab Republic.

Chen, C., Gao, Y., Li, Y., Bei, Y., 2022. Structure tensor-based interpolation for the derivation of accurate digital elevation models. Catena 208, 105733. https://doi.org/10.1016/j.catena.2021.105733.

Colombo, S., Calatrava-Requena, J., Hanley, N., 2003. The economic benefits of soil erosion control: An application of the contingent valuation method in the Alto Genil basin of southern Spain. J. Soil Water Conserv. 6, 367–373.

De Graaff, J., Eppink, L.A.A.J., 1999. Olive oil production and soil conservation in southern Spain, in relation to EU subsidy policies. Land Use Policy 16, 259–267. https://doi.org/10.1016/S0264-8377(99)00022-8.

Eitel, J.U.H., Williams, C.J., Vierling, L.A., Al-Hamdan, O.Z., Pierson, F.B., 2011. Suitability of terrestrial laser scanning for studying surface roughness effects on concentrated flow erosion processes in rangelands. Catena 87, 398–407. https://doi.org/10.1016/j.catena.2011.07.009.

Erdogan, S., 2009. A comparision of interpolation methods for producing digital elevation models at the field scale. Earth Surf Process Landf 34, 366–376. https://doi.org/10.1002/esp.1731.

Evrard, O., Bielders, C.L., Vandaele, K., van Wesemael, B., 2007. Spatial and temporal variation of muddy floods in central Belgium, off-site impacts and potential control measures. Catena 70, 443–454. https://doi.org/10.1016/j.catena.2006.11.011.

Falivene, O., Cabrera, L., Tolosana-Delgado, R., Sáez, A., 2010. Interpolation algorithm ranking using cross-validation and the role of smoothing effect. A coal zone example. Comput. Geosci. 36, 512–519. https://doi.org/10.1016/j.cageo.2009.09.015.

FAO and IUSS, 2015. World reference base for soil resources 2014: International soil classification system for naming soils and creating legends for soil maps – Update 2015, World Soil Resources Reports. FAO, Rome, Italy.

FAO 2015. State World Resource Soil. Technical Summary. Food and Agriculture Organization of the United Nations. Intergovernmental soil technical group. Available online at: https://www.icia.es/icia/download/Agroecolog%C3%ADa/Material/Estado_suelo.pdf.

FAOSTAT, 2016. Food and Agriculture Organization of the United Nations, Available online at: http://www.fao.org/faostat/es/#data/QC (accessed on 11 April 2023).

Fernández, T., Pérez, J.L., Cardenal, J., Gómez, J.M., Colomo, C., Delgado, J., 2016. Analysis of landslide evolution affecting olive groves using UAV and photogrammetric techniques. Remote Sens. (Basel) 8, 837. https://doi.org/10.3390/rs8100837.

Fernández, T., Pérez-García, J.L., Gómez-López, J.M., Cardenal, J., Calero, J., Sánchez-Gómez, M., Delgado, J., Tovar-Pescador, J., 2020. Multitemporal analysis of gully erosion in olive groves by means of digital elevation models obtained with aerial photogrammetric and LiDAR data. ISPRS Int. J. Geo Inf. 9, 260. https://doi.org/10.3390/ijgi9040260.

Fleskens, L., Stroosnijder, L., 2007. Is soil erosion in olive groves as bad as often claimed? Geoderma 141, 260–271. https://doi.org/10.1016/j.geoderma.2007.06.009.

Gao, C., Li, P., Hu, J., Yan, L., Latifi, H., Yao, W., Hao, M., Gao, J., Dang, T., Zhang, S., 2021. Development of gully erosion processes: A 3D investigation based on field scouring experiments and laser scanning. Remote Sens. Environ. 265, 112683 https://doi.org/10.1016/j.rse.2021.112683.

Gómez, J.A., Battany, M., Renschler, C.S., Fereres, E., 2003. Evaluating the impact of soil management on soil loss in olive orchards. Soil Use Manag. 19, 127–134. https://doi.org/10.1111/j.1475-2743.2003.tb00292.x.

Gómez J.A., Giráldez J.V., Fereres E., 2005. Water erosion in olive orchards in Andalusia (Southern Spain): a review. Geophysical Research Abstracts, 7 (2005), p. 08406 SRef-ID: 1607-7962/gra/EGU05-A-08406.

Gyssels, G., Poesen, J., Bochet, E., Li, Y., 2005. Impacto de las raíces de las plantas en la resistencia de los suelos a la erosión por el agua: una revisión. Progress in Physical Geography: Earth and Environment 29, 189–217. https://doi.org/10.1191/0309133305 pp443ra.

Habib, M., 2021. Evaluation of DEM interpolation techniques for characterizing terrain roughness. Catena 198, 105072. https://doi.org/10.1016/j.catena.2020.105072.

INE, 2009. National Institute of Statistics of Spain. Agrarian Census. 2009. Available online at: https://www.ine.es/dyngs/INEbase/es/operacion.htm?c=Estadistica_C&cid=1254736176851&menu=resultados&secc=1254736194950&idp=1254735727106 (accessed on 11 April 2023).

Infante-Amate, J., 2011. Ecología e historia del olivar andaluz. Un Estudio Socioambiental De La Especialización Olivarera En El Sur De España. 1750–2000.

Jiménez-Jiménez, S.I., Ojeda-Bustamante, W., Marcial-Pablo, M.J., Enciso, J., 2021. Modelos digitales del terreno generados con fotogrametría UAV de bajo costo: metodología y precisión. ISPRS Int. J. Geo-Inf. 10, 285. https://doi.org/10.3390/ijgi10050285.

Koci, J., Jarihani, B., Leon, J.X., Sidle, R.C., Wilkinson, S.N., Bartley, R., 2017. Assessment of UAV and Ground-Based Structure from Motion with Multi-View Stereo Photogrammetry in a Gullied Savanna Catchment. ISPRS Int. J. Geo-Inf. 6, 328. https://doi.org/10.3390/ijgi6110328.

Kraushaar, S., Herrmann, N., Ollesch, G., Vogel, H.-J., Siebert, C., 2014. Mound measurements — quantifying medium-term soil erosion under olive trees in Northern Jordan. Geomorphology 213, 1–12. https://doi.org/10.1016/j.geomorph.2013.12.021.

Li, J., Heap, A.D., 2014. Spatial interpolation methods applied in the environmental sciences: A review. Environ. Model. Softw. 53, 173–189. https://doi.org/10.1016/j.envsoft.2013.12.008.

Lima, F., Gómez Moreno, M.L., Blanco Sepúlveda, R., 2017. El olivar de montaña y la conservación del suelo en la transición de la economía orgánica a la industrial: el caso de Sierra de las Nieves (Málaga), 1940–1975. Ager. Revista De Estudios Sobre Despoblación y Desarrollo Rural 97–128. https://doi.org/10.4422/ager.2017.05.

Lima, F., Blanco Sepúlveda, R., Gómez Moreno, M.L., 2018. Soil erosion and environmental regulations in the European agrarian policy for olive groves (Olea europaea) of southern Spain [WWW Document]. accessed 13.4.23 Agrociencia 52 (3). https://www.scielo.org.mx/scielo.php?pid=S1405-31952018000300293&script=sci_abstract&tlng=en.

Lima, F., Gómez Moreno, M.L., Blanco Sepúlveda, R., 2021. Evolución del ajuste entre patrón de localización del olivar y capacidad agrológica en la montaña mediterránea andaluza (1956–2007). El caso de Sierra de las Nieves: respuestas locales a factores globales. Cuadernos Geográficos 60, 253–276. https://doi.org/10.30827/cuadgeo.v60i3.18095.

Lima, F., 2022. Desarrollo de métodos geo-espaciales de evaluación y seguimiento de las medidas de carácter medioambiental de la Política Agraria Común (PAC) en relación al control de la erosión hídrica del suelo. Aplicación en explotaciones de olivar de montaña de la provincia de Málaga. https://riuma.uma.es/xmlui/bitstream/handle/10630/24367/TD_LIMA_CUETO_Francisco_Javier.pdf?sequence=1&isAllowed=y.

Liu, K., Ding, H., Tang, G., Na, J., Huang, X., Xue, Z., Yang, X., Li, F., 2016. Detection of Catchment-Scale Gully-Affected Areas Using Unmanned Aerial Vehicle (UAV) on the Chinese Loess Plateau. ISPRS Int. J. Geo-Inf. 5, 238. https://doi.org/10.3390/ijgi5120238.

Liu, H., Qian, F., Ding, W., Gómez, J.A., 2019. Using 3D scanner to study gully evolution and its hydrological analysis in the deep weathering of southern China. Catena 183, 104218. https://doi.org/10.1016/j.catena.2019.104218.

López-Cuervo S., 1990. La erosión en los suelos agrícolas y forestales de Andalucía. Colección Congresos y Jornadas N° 17/1990. Consejería de Agricultura y Pesca, Junta de Andalucía.

Lu, H., Moran, C.J., Sivapalan, M., 2005. A theoretical exploration of catchment-scale sediment delivery. Water Resour. Res. 41 https://doi.org/10.1029/2005WR004018.

Lu, G.Y., Wong, D.W., 2008. An adaptive inverse-distance weighting spatial interpolation technique. Comput. Geosci. 34 (9), 1044–1055.

Lucieer, A., de Jong, S.M., Turner, D., 2014. Mapping landslide displacements using Structure from Motion (SfM) and image correlation of multi-temporal UAV photography. Progress in Physical Geography: Earth and Environment 38, 97–116. https://doi.org/10.1177/0309133313515293.

Mancini, F., Dubbini, M., Gattelli, M., Stecchi, F., Fabbri, S., Gabbianelli, G., 2013. Using Unmanned Aerial Vehicles (UAV) for High-Resolution Reconstruction of Topography: The Structure from Motion Approach on Coastal Environments. Remote Sens. 5, 6880–6898. https://doi.org/10.3390/rs5126880.

Martínez-Casasnovas, J.A., Ramos, M.C., Ribes-Dasi, M., 2002. Soil erosion caused by extreme rainfall events: mapping and quantification in agricultural plots from very detailed digital elevation models. Geoderma 105 (1-2), 125–140.

Meinen, B.U., Robinson, D.T., 2020. Mapping erosion and deposition in an agricultural landscape: Optimization of UAV image acquisition schemes for SfM-MVS. Remote Sens. Environ. 239, 111666 https://doi.org/10.1016/j.rse.2020.111666.

Papiernik, S.K., Schumacher, T.E., Lobb, D.A., Lindstrom, M.J., Lieser, M.L., Eynard, A., Schumacher, J.A., 2009. Soil properties and productivity as affected by topsoil movement within an eroded landform. Soil Tillage Res. 102, 67–77. https://doi.org/10.1016/j.still.2008.07.018.

Pereira, L.C., dos Santos, G.R., Marques, E.A.G., Pires, J.D., Renó, R., 2022. Construction of multidimensional geomechanical models with IDW and using R language. J. S. Am. Earth Sci. 116, 103775 https://doi.org/10.1016/j.jsames.2022.103775.

Peter, K.D., d'Oleire-Oltmanns, S., Ries, J.B., Marzolff, I., Ait Hssaine, A., 2014. Soil erosion in gully catchments affected by land-levelling measures in the Souss Basin, Morocco, analysed by rainfall simulation and UAV remote sensing data. Catena 113, 24–40. https://doi.org/10.1016/j.catena.2013.09.004.

Pineux, N., Lisein, J., Swerts, G., Bielders, C.L., Lejeune, P., Colinet, G., Degré, A., 2017. Can DEM time series produced by UAV be used to quantify diffuse erosion in an agricultural watershed? Geomorphology 280, 122–136. https://doi.org/10.1016/j.geomorph.2016.12.003.

Ramos, M.I., Feito, F.R., Gil, A.J., Cubillas, J.J., 2008. A study of spatial variability of soil loss with high resolution DEMs: A case study of a sloping olive grove in southern Spain. Geoderma 148, 1–12. https://doi.org/10.1016/j.geoderma.2008.08.015.

Scheidel, A., Krausmann, F., 2011. Diet, trade and land use: a socio-ecological analysis of the transformation of the olive oil system. Land Use Policy 28, 47–56. https://doi.org/10.1016/j.landusepol.2010.04.008.

Taguas, E.V., Gómez, J.A., 2015. Vulnerability of olive orchards under the current CAP (Common Agricultural Policy) regulations on soil erosion: a study case in Southern Spain. Land Use Policy 42, 683–694.

Van Oost, K., Van Muysen, W., Govers, G., Deckers, J., Quine, T.A., 2005. From water to tillage erosion dominated landform evolution. Geomorphology 72, 193–203. https://doi.org/10.1016/j.geomorph.2005.05.010.

Vanwalleghem, T., Laguna, A., Giráldez, J.V., Jiménez-Hornero, F.J., 2010. Applying a simple methodology to assess historical soil erosion in olive orchards. Geomorphology 114, 294–302. https://doi.org/10.1016/j.geomorph.2009.07.010.

Vanwalleghem, T., Amate, J.I., de Molina, M.G., Fernández, D.S., Gómez, J.A., 2011. Quantifying the effect of historical soil management on soil erosion rates in Mediterranean olive orchards. Agr. Ecosyst. Environ. 142, 341–351. https://doi.org/10.1016/j.agee.2011.06.003.

Verheijen, F.G.A., Jones, R.J.A., Rickson, R.J., Smith, C.J., 2009. Tolerable versus actual soil erosion rates in Europe. Earth Sci. Rev. 94, 23–38. https://doi.org/10.1016/j.earscirev.2009.02.003.

Wise, S.M., 2007. Effect of differing DEM creation methods on the results from a hydrological model. Comput. Geosci. Spatial Analysis 33, 1351–1365. https://doi.org/10.1016/j.cageo.2007.05.003.

Wong, D. W. S., 2017. Interpolation: Inverse-distance weighting. International Encyclopedia of Geography People the Earth Environment and Technology. doi: 10.1002/9781118786352.wbieg0066.

Yang, S., Guan, Y., Zhao, C., Zhang, C., Bai, J., Chen, K., 2019. Determining the influence of catchment area on intensity of gully erosion using high-resolution aerial imagery: A 40-year case study from the Loess Plateau, northern China. Geoderma 347, 90–102. https://doi.org/10.1016/j.geoderma.2019.03.042.

Zhang, J.H., Wang, Y., Jia, L.Z., Zhang, Z.H., 2017. An interaction between vertical and lateral movements of soil constituents by tillage in a steep-slope landscape. Catena 152, 292–298. https://doi.org/10.1016/j.catena.2017.01.030.

Zhang, J., Yang, M., Deng, X., Liu, Z., Zhang, F., 2019. The effects of tillage on sheet erosion on sloping fields in the wind-water erosion crisscross region of the Chinese Loess Plateau. Soil Tillage Res. 187, 235–245. https://doi.org/10.1016/j.still.2018.12.014.